

# European VLBI Network observations of fourteen GHz-Peaked-Spectrum radio sources at 5 GHz

L. Xiang<sup>1</sup>, C. Reynolds<sup>2</sup>, R. G. Strom<sup>3</sup>, and D. Dallacasa<sup>4,5</sup>

<sup>1</sup> National Astronomical Observatories/Urumsu Observatory, CAS, 40-5 South Beijing Road, Urumsu 830011, PR China  
e-mail: liux@ms.xjb.ac.cn

<sup>2</sup> Joint Institute for VLBI in Europe, Postbus 2, 7990 AA Dwingeloo, The Netherlands  
e-mail: reynolds@jive.nl

<sup>3</sup> ASTRON, Postbus 2, 7990 AA Dwingeloo; and Astronomical Institute, University of Amsterdam, The Netherlands  
e-mail: strom@astron.nl

<sup>4</sup> Dipartimento di Astronomia, Università di Bologna, via Ranzani 1, I-40127 Bologna, Italy  
e-mail: danielle.dallacasa@unibo.it

<sup>5</sup> Istituto di Radioastronomia – INAF, via P. Gobetti 101, 40129 Bologna, Italy

Received 28 July 2005 / Accepted 30 December 2005

**Abstract.** We present the results of EVN polarization observations of fourteen GHz-Peaked-Spectrum (GPS) radio sources at 5 GHz. These sources were selected from bright GPS source samples and we aimed at finding Compact Symmetric Objects (CSOs). We have obtained full polarization 5 GHz VLBI observations of 14 sources providing information on their source structure and spectral indices. The results show that two core-jet sources 1433–040 and DA193, out of 14 GPS sources, exhibit integrated fractional polarizations of 3.6% and 1.0% respectively. The other 12 sources have no clear detection of pc-scale polarization. The results confirm that the GPS sources generally have very low polarization at 5 GHz. The sources 1133+432, 1824+271 and 2121–014 are confirmed as CSOs. Three new CSOs 0914+114, 1518+046 and 2322–040 (tentative) have been classified on the basis of 5 GHz images and spectral indices. The sources 1333+589, 1751+278 and 2323+790 can be classified either as compact doubles, and then they are likely CSO candidates or core-jet sources; further observations are needed for an appropriate classification; 0554–026, 1433–040 and 1509+054 are core-jet sources. In addition, we estimate that a component in the jet of quasar DA193 has superluminal motion of  $3.3 \pm 0.6 h^{-1}c$  in 5.5 years.

**Key words.** galaxies: active – quasars: general – radio continuum: galaxies

## 1. Introduction

Compact Symmetric Objects (CSOs) are of particular interest in the study of the physics and evolution of active galaxies as introduced in our previous papers (Xiang et al. 2002, 2005, hereafter paper I, II). A number of CSOs have been found to be very young radio sources with ages of several centuries (Fanti 2000; Polatidis & Conway 2003; Gugliucci et al. 2005). How and why the radio emission has been recently triggered is still a matter of debate. There is some evidence that the host galaxies of CSO radio sources may be in a final (or even post-) merger stage, but no sound conclusion can be drawn given the small number of known CSOs. A larger sample of CSOs and more detailed studies of their radio properties, to be compared with those of old and extended radio galaxies, are fundamental steps for a better understanding of this phenomenon.

Models have been proposed to explain the evolution of individual small and young radio galaxies: their radio emission

grows in a self-similar way whereby the small CSOs become the extended radio galaxies about 3 orders of magnitude larger and about 4 orders of magnitude older than CSOs (e.g. Fanti et al. 1995; Readhead et al. 1996; Snellen et al. 2000). Support for this hypothesis has been found by Owsianik & Conway (1998) who reported on the detection of outward motion of the hot-spots of a few CSOs, and by Murgia et al. (1999) who found that the radiative ages of small sources are consistent with a young age.

CSOs have their radio axes roughly on the plane of the sky and are generally associated with elliptical galaxies. As a consequence of Doppler dimming, their jets are generally very rarely observed in this case, and the morphology is characterized by two bright lobes, possibly hosting hot-spots. Given their small size either Synchrotron Self-Absorption (SSA) or Free-Free absorption (FFA) or both take place, producing the typical peaked radio spectrum around 0.3–10 GHz in the observer’s frame. GHz-Peaked Spectrum (GPS) sources are also objects where HI absorption at the host redshift has been fre-

quently found (e.g. Vermeulen et al. 2003). In the case where the radio axis is aligned to the line of sight, the typical radio structure is a one-sided core-jet with Doppler boosting responsible for the amplification of the approaching side of the radio source.

Compact two-sided sources have been found in samples based on the spectral shape: CSOs are in the Pearson & Readhead (PR, 1988) and in the Caltech-Jodrell Bank (e.g. CJ-1; Xu et al. 1995) surveys of flat spectrum sources where the spectral peak is between the two frequencies used to define the source spectrum. Similar work has been done by Taylor & Peck (2003). In a flux-limited complete sample such as PR+CJ1 (200 sources with  $S_{5\text{GHz}} > 0.7$  Jy and  $\delta > 35^\circ$ ) 14 sources have been classified as CSOs. Among them, 10 also fulfill the definition of GPS sources. It is therefore efficient to search for CSOs in GPS samples (see paper I, II). GPS sources share the same properties as CSOs: they are generally smaller than 1 kpc and are young radio sources (Murgia 2003).

GPS radio sources make up a significant fraction of the bright radio source sample ( $\approx 10\%$ ) but they are not well understood. The GPS sources are powerful ( $P_{1.4\text{GHz}} \geq 10^{25} \text{W Hz}^{-1}$ ), compact ( $\leq 1$  kpc), and have convex radio spectra. Only about 18% (Stanghellini et al. 2005) of GPS sources show extended radio emission ( $> 1$  kpc), and it is diffuse and very faint, possibly the relic of an earlier radio activity. Most GPS sources appear to be truly compact and isolated (O’Dea 1998).

GPS radio galaxies show very low polarization (about 0.2% at 5 GHz, O’Dea 1998). The low integrated polarization may originate in a medium with a large Faraday depth located around the radio source. While the vast majority of GPS galaxies are found to be unpolarized at cm wavelengths, GPS quasars show relatively higher fractional polarization (Dallacasa 2004) consistent with (possibly slightly lower than) flat spectrum radio quasars. This implies that the galaxies are depolarized more than the quasars as is also expected (Cotton et al. 2003) in terms of Unified Scheme models. Higher frequency observations are required to determine the differences between GPS galaxies and quasars in polarization. The very low level of polarization often makes it difficult to measure reliable Rotation Measures (RMs) in GPS galaxies. The few sources with such measurements possess large RM values.

“Bright” GPS source samples (de Vries et al. 1997, Stanghellini et al. 1998) comprise a few tens of objects, and a couple of them either have never been imaged with VLBI or possess low dynamic range images. From the aforementioned samples, we have observed 22 sources in a number of VLBI projects carried out with the EVN (European VLBI Network): paper I reports on the first observing run (1999 November 13 at 1.6 GHz and 2000 May 29 at 2.3/8.4 GHz) while paper II reports on the second session (2002 July 4 at 2.3/8.4 GHz). From the multi-frequency VLBI images five CSOs and nine CSO candidates have been found.

In these follow up observations at 5 GHz, we aim at higher dynamic range imaging of the GPS sources, to confirm the CSO candidates found in earlier papers, to find new CSOs from the forementioned bright GPS samples, and, possibly, to measure the linear polarization. Our search for CSOs from the GPS samples is complementary to that by the COINS group (Taylor &

Peck 2003): there the search for CSOs is based on samples consisting mainly of flat spectrum radio sources, although also a GPS may appear as a flat or even inverted spectrum object if the peak flux density occurs close to the highest frequency of the selection.

## 2. Observations and data reduction

The observations were carried out on 30 October 2004 at 5 GHz using the MK5 recording system with a bandwidth of 16 MHz and sample rate of 128 Mbps in dual circular polarization. The EVN antennae in this experiment were Effelsberg, Westerbork (phased array), Jodrell, Medicina, Noto, Onsala, Torun, Hartebeesthoek, Urumqi and Shanghai. All stations contributed useful fringes. Snapshot observations of 14 sources (see Table 1) in a total of 24 hours were done. The calibration sources OQ208 and DA193 were observed with three 6-minute scans each. Most target sources were observed in more than ten 6-minute scans. The data correlation was completed at JIVE in March 2005.

Data from the Westerbork Synthesis Radio Telescope (WSRT) taken in parallel with the EVN session were processed to determine integrated properties for all the sources (including the source 3C48). The data were reduced in a standard way using the local NEWSTAR reduction package. All the target sources were found pointlike at the WSRT resolution ( $\sim 5''$ ) and their total flux densities are reported in Table 2.

The total flux densities of some sources were also measured shortly after the VLBI experiment in Effelsberg (5 sources; 3C286 was observed with 7.4 Jy). These values are listed in Table 1 as well.

Examination of the WSRT visibilities demonstrated that the array had been phased up well, so no further calibration was required to process the data. The calibrator OQ208 (believed to be unpolarized) was used to determine the instrumental polarization characteristics of each element in the array (dipole setting error and ellipticity). For each source, the Stokes parameters  $I$ ,  $Q$ ,  $U$  and  $V$  were determined from maps. The values for Stokes  $I$  have been scaled to the flux density of 3C48 (taken to be 5.48 Jy). Stokes  $Q$ ,  $U$  and  $V$  were used to determine the degree of linear polarization,  $m$  ( $= (Q^2 + U^2)^{0.5}/I$ ), and position angle of the electric vector (EVPA),  $\chi$  ( $= \frac{1}{2} \arctan(U/Q)$ ). The degree of circular polarization,  $m_V$  ( $= V/I$ ), was also measured.

For most of the target sources observed, the degree of polarization was found to be small, as has been seen in GPS sources in the past (O’Dea 1998). Examination of the  $m$  values for all sources showed that the majority had a degree of polarization near 0.6%, and with similar values of  $\chi$ . It seems most likely that the majority of weakly-polarized sources would cluster around  $m = 0$ , so it was concluded that the polarization of OQ208 in our measurement is not exactly zero. The polarization data were thus recalibrated using the average  $m$  (0.6%) and  $\chi$  ( $85^\circ$ ) found above, and these were taken to be definitive. The values for 15 sources can be found in Table 2. The probable error in  $m$ , based upon internal consistency and experience with the WSRT as a polarimeter, is estimated to be  $\pm 0.4\%$ ; the error in  $\chi$  (Table 2) depends upon this and the measured value of  $m$  (no value of  $\chi$  is given where the error is twice  $m$  or more).

Practically all of the circular polarization ( $m_V$ ) values measured are consistent with there being no significant circular polarization in these sources. The value we find for OQ208 is consistent with the upper limit established by Homan, Attridge and Wardle (2001).

### 2.1. The VLBI data

The Astronomical Image Processing System (AIPS) has been used for editing, *a priori* calibration, fringe-fitting, self-calibration and imaging of the VLBI data. The polarization calibration was carried out following the standard procedure in AIPS. The instrumental polarization was removed by LPCAL run on OQ208 which was assumed to be unpolarized and compact on a subset of baselines. The polarization angles on the VLBI images were calibrated by comparing the DA193 polarization angle in the integrated VLBI data with that of the Westerbork interferometric data, taken simultaneously to the VLBI observation. The correction was subsequently checked by comparing the WSRT and VLBI observations of the target source 1433–040 which gave a results agreeing within a few degrees. The Westerbork data were in turn checked using observations of 3C 48 which was measured to have an EVPA of  $115^\circ$ , in reasonable agreement with an Effelsberg single-dish result of  $104^\circ$  for 3C 48 observed at 4.85 GHz on 7 October 2004 (W. Reich, private commun.).

## 3. Results and comments on individual sources

Results from the 5 GHz VLBI observations are presented in this section. Basic information and some total flux densities of the sources appear in Table 1, the integrated properties of the sources from the WSRT data appear in Table 2, the parameters derived from the VLBI images are summarized in Table 3. We comment on the results for each source and then give a short discussion. We use  $S \propto \nu^{-\alpha}$  in this paper to define the spectral index.

### 3.1. 0552+398 (DA193, NVSS J055530+394848, WMAP 100)

The low-polarization quasar DA193 is a non-blazar source associated with an X-ray source 1WGA J0555+3948, and has been classified as a GPS source (Stanghellini et al. 1998) with a spectral turnover at 9.5 GHz. This radio loud quasar is extremely compact, is only resolved with VLBI, and is often used as a VLBI calibrator. The total intensity ( $I$ ) map at 5 GHz (Fig. 1) clearly shows a core and a jet. The core is very compact with about 70% of the total flux density, the jet component is also compact with about 30% of the total flux density. The jet position angle is  $-48^\circ$  in the north-west direction, roughly consistent with  $-53^\circ$  in a VSOP map at 5 GHz (Scott et al. 2004). The distance between the jet component and the core is 2.1 mas in our 5 GHz VLBI observation, which is greater than the 0.7 mas in the previous VSOP image. If the component detected here is the same as that detected in the VSOP image, then the increase over about 5.5 years corresponds to an apparent velocity of  $3.3 \pm 0.6 h^{-1}c$ . It has previously been suggested

that the jet has a superluminal motion of about  $2.2 \pm 0.7 h^{-1}c$  (Lister & Marscher 1998). The source is known to have relatively smooth flux density variability; the 5 GHz flux density has varied from 6.31 Jy (Stanghellini et al. 1998) to 5.23 Jy in this observation. At the epoch of the VSOP result (observed in March 1999) the core and the jet flux densities are 4.72 Jy and 2.57 Jy respectively, giving a total of 7.29 Jy if they were not over-estimated. So the jet has advanced with decreasing flux and keeping almost the same PA from March 1999 to October 2004. The VLA/VLBA monitoring data from 1999 to 2005 are decreasing for DA193 from 6.3 Jy to 5.1 Jy at 5 GHz.

The polarization VLBI image shows a weak feature, with integrated fractional polarization of 1% and  $\chi = 149^\circ \pm 9^\circ$  ( $-31^\circ \pm 9^\circ$ ). The fractional polarization measured at the WSRT is 1.3%. If we consider the integrated values measured at the VLA at various frequencies ranging from 5.0 to 43 GHz ([www.vla.nrao.edu/astro/calib/polar/](http://www.vla.nrao.edu/astro/calib/polar/)), it is clear that the fractional polarization is generally of the order of 1% or slightly higher with a substantial amount of Faraday Rotation, although it is difficult to estimate.

### 3.2. PKS 0554–026 (NVSS J055652–024105)

The 5 GHz VLBI image shows a compact core, with a jet or diffuse emission within 20 pc (Fig. 3). The total flux density measured at the WSRT has been fully accounted for in this image. The total flux density has decreased from 290 mJy (observed 1980, Wright & Otrupcek, 1990; Parkes Catalogue) to 171 mJy in this observation, indicating the source is variable and that the structure has to be interpreted in terms of a core-jet. The structure at 5 GHz is similar to that found at 2.3/8.4 GHz (paper II) in general. There is no clear detection of polarized flux.

### 3.3. 0914+114 (PKS 0914+11, NVSS J091716+111336)

The 5 GHz VLBI image (Fig. 4) exhibits a symmetric double source, with hints of a “tail” associated with the eastern lobe. From the relative separation between two main components detected in the 5 GHz VLBI image, it is clear that they correspond to components ‘A’ and ‘C’ in paper II. An upper limit of  $4.3 \pm 1.9$  mJy may be associated at the position of component ‘B’ while it seems there is no likely detection at the position of component ‘D’ (paper II). Here we tentatively register the single component at 8.4 GHz (it was assumed to be component ‘C’ in paper II) as component ‘A’ in the 5 GHz image by considerations based on its spectrum. Such an identification means that the spectral indices of both components ‘A’ and ‘C’ between 5 and 8.4 GHz are steeper than between 2.3 and 5 GHz (Fig. 5), which is typical of the components in CSOs above the turnover frequency. In this case component ‘A’ has a flat spectrum ( $\alpha = 0.09$ ) between 2.3 and 5 GHz and this allows its detection at 8.4 GHz, while component ‘C’ would have a rather steep spectrum between 2.3 and 5 GHz and then it could reasonably be expected to be undetected at 8.4 GHz. The possibility that the single component detected at 8.4 GHz has to

**Table 1.** GPS sources. Columns 1 through 13 provide source name, optical identification (G: galaxy, Q: quasar, EF: empty field), optical magnitude (‘V’, ‘R’ are the bands in the optical, ‘r’ band–defined by Stanghellini et al. 1993), redshift (those with \* are a photometric estimate by Heckman et al. 1994), linear scale factor pc/mas [ $H_0 = 100 h \text{ km s}^{-1} \text{ Mpc}^{-1}$  and  $q_0 = 0.5$  have been assumed], maximum VLBI angular size from paper I, II or this observation, maximum VLBI linear size, 5 GHz total flux density measured at Effelsberg, low frequency spectral index, high frequency spectral index, turnover frequency, peak flux density and references for the spectral information (ref: 1, de Vries et al. 1997; 2, Stanghellini et al. 1998; 3, Dallacasa et al. 2000; 4, O’Dea et al. 1996; 5, Spoelstra et al. 1985).

1	2	3	4	5	6	7	8	9	10	11	12	13
source	<i>id</i>	<i>mag</i>	<i>z</i>	<i>pc/mas</i>	$\theta$	<i>L</i>	$S_{\text{EF}}$	$\alpha_l$	$\alpha_h$	$\nu_m$	$S_m$	ref
					[mas]	[pc]	[Jy]			[GHz]	[Jy]	
0554–026	G	18.5V	0.235	$2.37h^{-1}$	30	$71h^{-1}$		-1.07	0.63	1.0	0.8	1
0914+114	G	20.0r	0.178	$1.95h^{-1}$	150	$293h^{-1}$	0.11	-0.1	1.6	0.3	2.3	2
1133+432	EF				40		0.45	-0.60	0.6	1.0	1.4	1
1333+589	EF				20		0.67	-0.84	0.52	4.9	0.73	3
1433–040	G	22.3r			20							4,5
1509+054	G	16.2V	0.084	$1.06h^{-1}$	17	$18h^{-1}$		-1.72	0.46	11	0.77	3
1518+046	Q	22.2R	1.296	$4.3h^{-1}$	160	$688h^{-1}$	1.06	-0.6	1.3	0.9	4.58	2
1751+278	G	21.7R	0.86*	$4.2h^{-1}$	50	$210h^{-1}$		-0.27	0.57	1.4	0.6	1
1824+271	G?	22.9R			45			-0.39	0.75	1.0	0.4	1
2121–014	G	23.3R	1.158	$4.3h^{-1}$	88	$378h^{-1}$		-0.56	0.75	0.5	1.8	1
2322–040	G	23.5R			65			-0.42	0.75	1.4	1.3	1
2323+790	G	19.5V			32		0.43	-0.3	0.75	1.4	1.2	1
DA193	Q	18.0V	2.365	$4.0h^{-1}$	4	$16h^{-1}$		-1.6	0.6	9.5	7.8	2
OQ208	G	14.6r	0.077	$1.0h^{-1}$	10	$10h^{-1}$		-1.5	1.6	4.9	2.76	2

**Table 2.** Integrated properties of the sources from the WSRT data, values of  $\chi$  are likely to be meaningless for objects with  $m \leq 0.4\%$ .

1	2	3	4	5
source	<i>I</i>	<i>m</i>	$\chi \pm \sigma_\chi$	$m_V$
	[mJy]	[%]	[°]	[%]
0554–026	$171 \pm 6$	0.3	$18 \pm 43$	0.1
0914+114	$118 \pm 9$	0.4	$94 \pm 33$	0.1
1133+432	$480 \pm 15$	0.2	-	-0.0
1333+589	$720 \pm 42$	0.4	$141 \pm 30$	-0.0
1433–040	$246 \pm 15$	3.8	$134 \pm 5$	-0.3
1509+054	$688 \pm 63$	0.7	$173 \pm 17$	0.1
1518+046	$994 \pm 52$	0.7	$176 \pm 17$	0.0
1751+278	$260 \pm 12$	0.3	$164 \pm 41$	-0.1
1824+271	$111 \pm 5$	0.3	-	-0.0
2121–014	$327 \pm 13$	0.4	$29 \pm 30$	0.0
2322–040	$548 \pm 15$	0.1	-	-0.1
2323+790	$438 \pm 27$	0.5	$93 \pm 25$	-0.0
3C48	$5480 \pm 50$	3.1	$115 \pm 5$	-0.0
DA193	$5232 \pm 64$	1.3	$149 \pm 9$	0.1
OQ208	$2609 \pm 15$	0.6	$175 \pm 19$	0.0

be associated with component ‘B’ in paper II, is ruled out by the upper limit of 4.3 mJy found in the present data. Because component ‘B’ has a flat spectrum of  $\alpha = 0.23$  between 2.3 and 8.4 GHz.

From the inverted spectra of the components and their symmetrical structure, we classify the source as a CSO. The total flux density has decreased from 140 mJy (observed 1979, Parkes Catalogue 1990) to 118 mJy in this observation. For our observations from 2.3/8.4 GHz to 5 GHz separated by 2.4 years, source variability may have influenced the spectral index estimates, but the error introduced by this should be small

comparing to the long term variation of  $\sim 16\%$ . The total flux density at 5 GHz is recovered in the VLBI image. No polarization is detected in the 5 GHz VLBI observation.

### 3.4. 1133+432 (NVSS J113555+425844)

This is an empty field ( $> 23 \text{ mag}$ ) in the optical (Stickel & Kühr, 1994). The 5 GHz VLBI image (Fig. 6) shows a double source. The double structure exhibits two opposite edge-brightened hotspot/lobes with spectral indices of 1.1 and 1.4 between 2.3 and 5 GHz for the northern and southern lobe re-

**Table 3.** Parameters of the components in the VLBI images at 5 GHz. The columns give: (1) source name and possible classification (CSOc: Compact Symmetric Object candidate, cj: core-jet); (2) total image intensity measured with IMEAN at 5 GHz; (3) component identification labeled to Xiang et al. 2002, 2005; (4),(5) peak (per beam) and integral intensity of component at 5 GHz measured with JMFIT; (6),(7) major/minor axes (with error  $\leq 10\%$ ) and position angle of component at 5 GHz measured with JMFIT; (8),(9) distance and position angle relative to the first component; (10) brightness temperature of component; (11) integrated fractional polarization in source.

1	2	3	4	5	6	7	8	9	10	11
Name class	$S_{vlbi}$ [mJy]		$S_p$ [mJy]	$S_{int}$ [mJy]	$\theta_1 \times \theta_2$ [mas]	$PA$ [ $^\circ$ ]	$d$ [mas]	[ $^\circ$ ]	$T$ [ $10^7 K^\circ$ ]	$m$ [%]
0554–026	175 $\pm$ 3	AB	50.8 $\pm$ 0.7	114.9 $\pm$ 2.1	7.1 $\times$ 3.0	0.1 $\pm$ 0.5	0		2.0	$\leq 0.4$
cj		C	17.6 $\pm$ 0.6	77.3 $\pm$ 3.4	10.7 $\times$ 3.9	70.4 $\pm$ 1.3	0.4 $\pm$ 0.1	–69.7 $\pm$ 4.7	0.6	
0914+114	116 $\pm$ 2	A	27.2 $\pm$ 0.8	43.0 $\pm$ 2.0	6.5 $\times$ 3.3	0.6 $\pm$ 1.8	0		0.6	
CSO		B		$\leq 4.3 \pm 1.9$						
		tail		20 $\pm$ 1.3						
		C	25.2 $\pm$ 0.8	46.1 $\pm$ 2.2	6.7 $\times$ 3.7	4.1 $\pm$ 2.1	84.3 $\pm$ 0.1	81.4 $\pm$ 0.1	0.6	
		D		$\leq 3.8 \pm 1.5$						
1133+432	416 $\pm$ 11	A		290 $\pm$ 14						
CSO		B1	44.5 $\pm$ 0.4	67.4 $\pm$ 0.9	3.2 $\times$ 2.1	35.3 $\pm$ 0.8	0			
		B2	25.5 $\pm$ 0.4	53.3 $\pm$ 1.1	3.3 $\times$ 2.8	106.8 $\pm$ 3.3	2.7 $\pm$ 0.1	1.3 $\pm$ 0.5		
1333+589	580 $\pm$ 55	N	288.5 $\pm$ 2.4	331.6 $\pm$ 4.5	3.4 $\times$ 3.2	45.1 $\pm$ 4.8	0			
CSOc/cj		S	182.0 $\pm$ 2.3	225.0 $\pm$ 4.7	3.7 $\times$ 3.2	125.7 $\pm$ 4.0	12.7 $\pm$ 0.1	197.5 $\pm$ 0.5		
1433–040	206 $\pm$ 10	core	66.5 $\pm$ 0.3	125.8 $\pm$ 0.8	6.1 $\times$ 2.8	177.8 $\pm$ 0.2	0			3.6
cj		jet	14.1 $\pm$ 0.3	67.7 $\pm$ 1.5	9.6 $\times$ 4.5	17.2 $\pm$ 0.9	1.4 $\pm$ 0.2	12.4 $\pm$ 3.5		3.6
1509+054		E	76.9 $\pm$ 1.5	108.3 $\pm$ 3.3	4.6 $\times$ 3.7	2.3 $\pm$ 3.5	0		2.0	
cj		W	389.0 $\pm$ 1.5	548.5 $\pm$ 3.3	4.9 $\times$ 3.5	1.5 $\pm$ 0.5	5.2 $\pm$ 0.1	–89.7 $\pm$ 0.4	10.2	
	682 $\pm$ 31	A	80.8 $\pm$ 1.5	91.8 $\pm$ 2.7	3.8 $\times$ 1.2	7.1 $\pm$ 0.5	0		6.5	
		B	317.3 $\pm$ 1.4	464.0 $\pm$ 3.2	4.2 $\times$ 1.4	7.4 $\pm$ 0.1	5.3 $\pm$ 0.1	–89.2 $\pm$ 0.1	25.2	$\leq 0.4$
		C	38.0 $\pm$ 1.4	92.8 $\pm$ 4.5	5.2 $\times$ 2.0	13.6 $\pm$ 1.3	7.6 $\pm$ 0.1	–81.6 $\pm$ 0.1	2.9	
		D	27.3 $\pm$ 1.4	33.2 $\pm$ 2.8	3.9 $\times$ 1.3	7.6 $\pm$ 1.6	10.4 $\pm$ 0.1	–97.1 $\pm$ 0.1	2.1	
1518+046	869 $\pm$ 9	A	135.4 $\pm$ 1.6	268.6 $\pm$ 4.4	6.7 $\times$ 3.9	1.9 $\pm$ 0.9	0		7.0	$\leq 0.5$
CSO/MSO		B	49.7 $\pm$ 1.6	108.9 $\pm$ 4.8	6.7 $\times$ 4.3	4.3 $\pm$ 2.9	10.4 $\pm$ 0.1	39.9 $\pm$ 0.1	2.6	
		C	205.6 $\pm$ 1.7	249.8 $\pm$ 3.3	5.2 $\times$ 3.1	178.9 $\pm$ 0.6	135.8 $\pm$ 0.1	206.7 $\pm$ 0.1	10.5	$\leq 0.5$
		D	97.0 $\pm$ 1.6	238.0 $\pm$ 5.2	8.0 $\times$ 4.1	23.1 $\pm$ 0.9	133.2 $\pm$ 0.1	207.0 $\pm$ 0.1	4.9	
1751+278	270 $\pm$ 10	A	163.4 $\pm$ 0.5	243.4 $\pm$ 1.1	5.3 $\times$ 3.5	175.4 $\pm$ 0.3	0		7.2	$\leq 0.4$
CSOc/cj		B	11.7 $\pm$ 0.8	20.6 $\pm$ 2.2	5.8 $\times$ 3.7	7.7 $\pm$ 6.6	23.3 $\pm$ 0.2	227.5 $\pm$ 0.1	0.5	
1824+271	115 $\pm$ 6	A	48.5 $\pm$ 0.2	74.3 $\pm$ 0.5	6.3 $\times$ 3.9	177.3 $\pm$ 0.4	0			
CSO		B	19.7 $\pm$ 0.2	31.4 $\pm$ 0.5	6.1 $\times$ 4.2	175.6 $\pm$ 1.1	21.6 $\pm$ 0.1	–82.6 $\pm$ 0.1		
2121–014	317 $\pm$ 9	A1	99.4 $\pm$ 0.8	154.2 $\pm$ 1.8	6.8 $\times$ 3.6	2.3 $\pm$ 0.5	0		4.0	
CSO		A2	8.3 $\pm$ 0.7	42.0 $\pm$ 4.3	9.8 $\times$ 8.3	33.0 $\pm$ 21.4	2.8 $\pm$ 0.7	57.4 $\pm$ 2.1	0.3	
		B	7.4 $\pm$ 0.8	13.3 $\pm$ 2.2	6.6 $\times$ 4.3	0.6 $\pm$ 11	16.8 $\pm$ 0.6	86.5 $\pm$ 1.8	0.3	
		C1	33.0 $\pm$ 0.9	33.7 $\pm$ 1.6	4.5 $\times$ 3.6	2.9 $\pm$ 4.6	60.8 $\pm$ 0.5	82.0 $\pm$ 0.4	13.4	
		C2	33.4 $\pm$ 0.8	73.7 $\pm$ 2.6	9.2 $\times$ 3.8	1.8 $\pm$ 1.0	61.4 $\pm$ 0.5	84.4 $\pm$ 0.4	13.5	
2322–040	560 $\pm$ 15	A	290.2 $\pm$ 1.5	429.1 $\pm$ 3.4	5.1 $\times$ 2.7	175.0 $\pm$ 0.3	0			
CSO		tail	24.4 $\pm$ 1.5	50.6 $\pm$ 4.2	7.2 $\times$ 2.6	3.7 $\pm$ 2.1	6.7 $\pm$ 0.2	192.5 $\pm$ 0.2		
		B	40.7 $\pm$ 1.5	78.3 $\pm$ 4.0	6.1 $\times$ 2.8	157.8 $\pm$ 1.7	37.3 $\pm$ 0.2	176.4 $\pm$ 0.2		
2323+790	409 $\pm$ 13	A1	73.6 $\pm$ 0.3	229.4 $\pm$ 1.3	9.9 $\times$ 3.7	10.8 $\pm$ 0.2	0			
CSOc/cj		A2	110.0 $\pm$ 0.3	123.0 $\pm$ 0.6	4.1 $\times$ 3.3	172.6 $\pm$ 0.5	0.2 $\pm$ 0.1	143.4 $\pm$ 1.2		
		B	30.3 $\pm$ 0.3	45.5 $\pm$ 0.7	4.8 $\times$ 3.7	25.0 $\pm$ 1.7	17.1 $\pm$ 0.1	–76.8 $\pm$ 0.1		
		C	8.7 $\pm$ 0.3	24.0 $\pm$ 1.1	7.8 $\times$ 4.2	9.3 $\pm$ 2.3	22.5 $\pm$ 0.2	–77.5 $\pm$ 0.3		
DA193	5272 $\pm$ 172	core	3415 $\pm$ 7	3943 $\pm$ 13	3.8 $\times$ 1.5	22.7 $\pm$ 0.1	0		686.5	1.0
cj		jet	951 $\pm$ 7	1300 $\pm$ 14	3.8 $\times$ 1.8	21.2 $\pm$ 0.3	2.1 $\pm$ 0.1	–48.3 $\pm$ 0.1	191.0	1.0
OQ208	2656 $\pm$ 96	NE	1728 $\pm$ 7	2342 $\pm$ 16	4.7 $\times$ 2.8	3.3 $\pm$ 0.3	0		56.5	
CSO		SW	173 $\pm$ 7	236 $\pm$ 16	4.0 $\times$ 3.3	17.1 $\pm$ 9.3	6.5 $\pm$ 0.2	230.2 $\pm$ 0.2	5.7	

spectively, see Fig. 7. Orienti et al (2004) imaged the source with the VLBA at 5 GHz and they found a source structure very similar to our Fig. 6. We confirm that the source can be classified as a CSO. About 92% of the total flux density has

been recovered in our 5 GHz image. No polarization could be detected for this source.

### 3.5. 1333+589 (VCS1 J1335+5844, 4C +58.26)

It is an empty field ( $> 23$  mag) in the optical (Stickel & Kühr, 1994). The radio spectrum, typical of a GPS source, peaks at 4.9 GHz; the 5 GHz VLBI image shows a double structure (Fig. 8). Images at 2.3 and 8.4 GHz are available in paper I and the VLBA Calibrator Survey (VCS, part1, Beasley et al. 2002). The northern component appears more compact than the southern one, it may harbor a flat spectrum nucleus and it seems a jet is embedded in it; its flux density is the same as Xu et al. (1995) at 5 GHz. However, the southern component has a flux density of 225 mJy in our observation, about 30% less than in Xu et al. (1995), the deficit may be due to poor uv-coverage because the source has only 6 observing scans which are less than those for other target sources in our observations. The distance between the components ‘N’ and ‘S’ is 12.7 mas, the same as in Xu et al. (1995). Both components have an overall radio spectrum with the characteristic convex shape of self-absorbed regions (Fig. 9), and they can be interpreted in terms of the lobes of the source. The spectral shape is confirmed in more detail by higher frequency data (Oriente et al. 2006).

About 87% of the Effelsberg flux density has been accounted for in the VLBI image. No polarization is detected in the 5 GHz VLBI observation.

### 3.6. 1404+286 (OQ 208, Mrk 0668, NVSS J140700+282714)

Our image (Fig. 10) shows a structure which is similar to previous VLBI observations at 5 GHz. This is a CSO as confirmed by Stanghellini et al. (1998, 2000) and Lister et al. (2003). No polarization is detected in our 5 GHz VLBI observation. It was previously reported that its linear polarization is less than 0.2% at 5 GHz (Stanghellini et al. 1998). The source has been found to be a Compton-thick AGN in X-rays (Guainazzi et al. 2004); Yang & Liu (2005) suggest the presence of a dense medium capable of confining the radio source. The (ionized) medium may have then depolarized the radio emission.

### 3.7. 1433–040 (PKS 1433–04, J1435–0414)

The source is identified as a galaxy with  $m_r=22.3$  (Stanghellini et al. 1993). It can be found in O’Dea (1996) and in the early GPS sample list by Spoelstra (1985). The parsec scale morphology appears as a core-jet (Fig. 11), and the 2.3 GHz VLBI image from the VCS3 (VLBA calibrator survey 3, Petrov et al. 2005) clearly shows a core-jet structure oriented to the North-East. The 5 GHz image can be fitted with two Gaussian components, a central compact one, likely to be the core, and a weaker and broader one to the North-East with a separation of 1.4 mas and  $PA=12.4^\circ$ . The core-jet classification is supported by the positive detection of polarization in this source. Integrated polarization of 3.6% is detected in the 5 GHz VLBI observation, with an EVPA of  $143^\circ$  (Fig. 12). The polarization seems largely to come from the jet component because the polarized emission lies close to the jet position. We obtained a fractional polarization of 3.8% with an EVPA of  $134^\circ$  in the WSRT data for this source.

The radio spectrum of the source turns over around 1 GHz. The total flux density has increased from 200 mJy (observed 1980, Parkes Catalogue 1990) to 246 mJy in this observation. About 83% of the total flux density has been detected in the 5 GHz VLBI image.

### 3.8. 1509+054 (VCS2 1511+0518, JVAS J1511+0518)

This object has been identified with a Seyfert-1 galaxy at a redshift of 0.084 (Chavushyan et al. 2001). The 5 GHz VLBI image shows an asymmetric double (Fig. 13), which is similar to the 8.4 GHz image in paper I. The eastern component is more compact than the western one which is marginally resolved in (Fig. 13). The spectral indices of the eastern component and western part are -1.96 and 0.61 between 5 and 8.4 GHz (from Fig. 13 at 5 GHz and paper I at 8.4 GHz). From the compactness and steep rising spectrum, the component ‘A’ may harbor the core of the source. However, if we consider also the VCS data and higher frequency VLBA observations by Oriente et al. (2006), we can also interpret the source as dominated by two self-absorbed, micro hot-spots/lobes with slightly different turnover frequency.

The total flux density of the source has increased from 526 mJy (Dallacasa et al. 2000) to 688 mJy in this observation, suggesting it is variable and this is a core-jet source. Weak polarization is possibly detected in the central component (Fig. 14) in our 5 GHz VLBI image; we use it as an upper limit in Table 3, although the EVPA differs from that of the WSRT result. The source may be associated with the X-ray source 1WGA J1511.6+0518.

### 3.9. 1518+046 (VCS1 J1521+0430, 4C +04.51)

The 5 GHz VLBI image shows a classical double (Fig. 15), with two hotspots in the northern and tail/lobe in the southern part. The identification of these components as hotspots/lobes is supported by the spectra, as given in paper I (see also Dallacasa et al. 1998). The total flux density is stable from 1.03 Jy (Parkes Catalogue 1990) to 1.06 Jy in this observation. We conclude that this is a CSO or, possibly a MSO, given its size around 1 kpc. Possible polarization is detected at the hotspots in the 5 GHz image, we use it as an upper limit in Table 3, although the EVPA differs from that of the WSRT result.

### 3.10. 1751+278 (MG2 J175301+2750, JVAS 1753+2750)

The 5 GHz VLBI image exhibits asymmetric double structure. The northern component ‘A’ is about 10 times brighter than the southern one (Fig. 16). We derive a spectral index of 0.59 for component ‘A’ between 1.6 and 5 GHz. We could relate the weaker one at 5 GHz to component ‘B’ or ‘C’ or even both at 1.6 GHz because its separation of 23.3 mas from component ‘A’ at 5 GHz, is close both to the 22 mas separation of ‘B’ from ‘A’ and to the 23 mas separation of ‘C’ from ‘A’ (paper I) at 1.6 GHz. If it is ‘B’ its spectral index is 0.6, if it is ‘C’ then  $\alpha = -0.4$ , or it is a combination of ‘B’ and ‘C’ in which case

$\alpha = 0.8$ . Therefore, if the weaker component at 5 GHz is ‘B’ or ‘B+C’ at 1.6 GHz, the steep spectrum would suggest the source has a double lobe/hotspots; if it is ‘C’ then the resultant rising spectrum would indicate ‘C’ is the core of the source. The source is suggested to vary at 1.4 GHz, and may not be a genuine GPS source (paper I). At 5 GHz its total flux density has slightly changed from 280 mJy (Griffith et al. 1990) to 260 mJy in this observation, although this difference is consistent with no variability within  $1\sigma$ . However, further VLBI observations at other frequencies would be required to clarify the source classification. The total flux density at 5 GHz is recovered in the VLBI image. Possible polarization is detected at the strong component in the 5 GHz image, which we use as an upper limit in Table 3.

### 3.11. 1824+271 (MG2 J182632+2707)

The 5 GHz VLBI image (Fig. 17) shows a symmetric double structure, which is similar to 2.3/8.4 GHz images (paper II). The spectral indices for components ‘A’ and ‘B’ respectively are 1.0 and 0.8 between 2.3 GHz and 5 GHz while between 5 GHz and 8.4 GHz they both become steeper than  $\alpha = 1.0$  (Fig. 18), suggesting that the source structure can be interpreted in terms of a double-lobed object. We then confirm that the source is a CSO. The total flux density has slightly increased from 98 mJy (Griffith et al. 1990) to 111 mJy in this observation, although there is consistency with no flux density variability within  $1\sigma$ . The whole flux density has been accounted for in the VLBI image. No polarization is detected in the 5 GHz VLBI and WSRT observations.

### 3.12. 2121–014 (PKS 2121–01, NVSS J212339–011234)

The 5 GHz VLBI image shows two bright regions, likely the lobes, and an additional weaker feature, possibly the core or a knot in a jet, between them (Fig. 19). We estimated the spectral index of the core candidate between 2.3 GHz and 5 GHz by using the peak flux density of 45 mJy at 2.3 GHz and the measure from our data at 5 GHz, and it turns out to be very steep  $\alpha = 1.5$  (details are explained further down), unless dramatic flux density variability took place. In that case, it is more likely a fading knot in a jet or part of the tailed structure characteristic of the radio lobes, which is also consistent with the non detection at 8.4 GHz (paper II). In paper II, we fitted two Gaussian components ‘A’ and ‘B’ in one ‘tvwindow’ using the AIPS task JMFIT resulting in components ‘A’ and ‘B’ largely overlapping with a separation of 4 mas only (the value of separation is not listed in paper II). Here we refit components ‘A’ and ‘B’ at 2.3 GHz with single components in separate windows, which gives peak/beam and integrated flux density 275, 330 mJy for ‘A’ and 45, 120 mJy for ‘B’ respectively, with a separation of 16.0 mas between them which is consistent with the separation 16.8 mas measured at 5 GHz. With the remeasured data at 2.3 GHz, the spectral indices between 2.3 GHz and 5 GHz are 1.0, 0.7 for ‘C’, ‘A’ (we have combined components ‘C1’/‘C2’ into ‘C’, ‘A1’/‘A2’ into ‘A’ at 5 GHz).

For  $\alpha = 1.5$  of the ‘B’ component between 2.3 and 5 GHz, we have used the peak/beam flux instead of integrated flux at 2.3 GHz, with a comparable angular size to component ‘B’ at 5 GHz. From the double lobe-like features and their steep spectra (Fig. 20) we confirm the source is a CSO, although the ‘central’ component ‘B’ has not been confirmed as a core. The total flux density seems stable from 320 mJy (Parkes Catalogue 1990) to 327 mJy in this observation. No polarization is detected in the 5 GHz VLBI observation, and the WSRT value is similarly low.

### 3.13. PKS 2322–040 (NVSS J232510–034446)

With a typical GPS spectrum peaked at 1.4 GHz, the 5 GHz VLBI image exhibits double lobe/hotspots and a weak jet/tail-like emission to the northern component (Fig. 21). It seems similar to that at 2.3 GHz (paper II) where a sign of the jet might be embedded in component ‘A’ but not well resolved. Component ‘B’ assumes a lobe-like morphology in our image at 5 GHz. The spectral indices of components ‘A’, ‘B’ are 0.56, 1.41 respectively between 2.3 and 5 GHz (see also Fig. 22). The total flux density has increased by 10% from 500 mJy (Parkes Catalogue 1990) to 548 mJy in this observation. Based on the steep spectra and the radio structure, we tentatively classify the source as a CSO. No polarization is detected either in the 5 GHz VLBI or the WSRT observations.

### 3.14. 2323+790 (NVSS J232503+791715)

This object is classified as a galaxy (Stickel & Kühr 1996). On the large scale, the NVSS image exhibits two components separated by  $\sim 2$  arcmin. It is not clear whether they are separate sources. The WENSS map indicates the source has multiple components. On the very small scale, the 5 GHz VLBI image shows two components, both resolved; the easternmost is the brightest and has a North-South elongation, which is quite perpendicular to the major axis of the weaker western component. The overall structure can be classified as a double (Fig. 23). This is the first VLBI image for the source and we cannot provide a proper classification on its basis only. It belongs to the S5 catalogue, and the total flux density seems stable at 5 GHz from 448 mJy (S5 data, observed in 1978, Kühr et al. 1981) to 438 mJy in this observation. We consider this source as a CSO candidate, requiring further observations for a proper classification. About 93% of the total flux density has been detected in the VLBI image. No polarization is detected either in the 5 GHz VLBI or in the WSRT observation.

## 4. Discussion

CSOs are compact radio sources with relatively steep spectrum double lobes on the opposite sides of the core. Ideally, a core component with a spectrum flatter than the lobes must be identified before sources can be claimed to be a CSO. For some CSOs with a jet axis very close to the plane of the sky the core may be so weak as to be undetectable unless very high dynamic range images are available; yet a CSO identification can still be secure if there are quite symmetric, edge-brightened

lobes (Taylor & Peck 2003). Examples are the radio sources 0914+114, 1133+432, 1518+046, 1824+271, 2121–014 presented in this paper, for which the CSO classification can be proposed despite the failure to detect the core. These sources have resolved, steep spectrum components dominating the pc-scale radio emission. The long term ( $> 15$  years) variations as indicated in the last section are  $-16\%$ , unknown,  $+3\%$ ,  $+12\%$ , and  $+2\%$  respectively for the 5 target sources classified as CSOs. During the 2.4 years that elapsed between the present and our earlier observations their variations should not affect substantially their spectral indices and then their CSO classification can be considered secure.

The optical counterparts of the 14 sources in our sample are primarily galaxies (10), with the addition of 2 quasars and 2 empty fields. One quasar (DA193) and one galaxy (1433–040) show significant linear polarizations  $\geq 1\%$ , while there is marginal detection ( $\leq 0.5\%$ ) of polarized emission in the remaining quasar (1518+046) and 2 further galaxies (1509+054 and 1751+278). The remaining sources do not show any polarization.

These results are consistent with earlier work on the GPS sources, known to show very low or no polarization. They may have been largely depolarized by a dense ionized ambient medium characterized by small scale inhomogeneities in its magnetic field and in which the radio source is embedded. An example of such a medium can be found in DA193, known to have a very high rest-frame rotation measure ( $> 4700 \text{ rad m}^{-2}$ ; Lister & Marscher 1998), possibly responsible for some amount of Faraday depolarization as well. A similarly dense ionized medium surrounding the Compton-thick OQ208 (Guainazzi et al. 2004) may have led to undetectable radio polarization.

Given that in general the rotation measure is not or poorly known for GPS sources, no correction for the effect of Faraday rotation on intrinsic orientation of the electric vector ( $\chi$ ) has been applied in the images presented here, and therefore the intrinsic magnetic field vectors are not necessarily perpendicular to the *observed* electric vectors shown in the images.

## 5. Summary and Conclusions

1. We have obtained 5 GHz total intensity VLBI images for 14 GPS sources. The parameters of source structure and spectra have been derived, allowing, for a number of cases, a secure morphological classification.
2. Two core-jet sources (1433–040 and DA193) show integrated fractional polarization of 3.6% and 1.0% respectively. Three sources show possible weak polarization  $\leq 0.5\%$ , while the remaining nine sources are found to be unpolarized at 5 GHz, confirming that this is a characteristic property of GPS sources.
3. The sources 1133+432, 1824+271 and 2121–014 have been confirmed as CSOs, and three new CSOs have been classified as such on the basis of new evidence coming from the 5 GHz images and the spectral indices: they are 0914+114, 1518+046, and 2322–040.
4. The sources 1333+589, 1751+278 and 2323+790 which show double structure are likely candidate CSOs or core-

jet sources; further VLBI observations are required for their proper classification. 0554–026, 1433–040 and 1509+054 are classified as core-jet sources.

5. The jet component in the quasar DA193 has a superluminal motion of  $3.3 \pm 0.6 h^{-1}c$  in 5.5 years, confirming earlier results.

*Acknowledgements.* LX is grateful for support from the KNAW/CAS (Royal Dutch Academy of Sciences/Chinese Academy of Sciences) bilateral agreement. We thank Dave Graham for the total flux density measurement at Effelsberg. The European VLBI Network is a joint facility of European, Chinese, South African and other radio astronomy institutes funded by their national research councils. The WSRT is operated by ASTRON with financial support from the Netherlands Organization for Scientific Research (NWO). This research has made use of the NASA/IPAC Extragalactic Database (NED) which is operated by the Jet Propulsion Laboratory, Caltech, under contract with NASA. Parkes Catalogue (1990) was made by Australia Telescope National Facility.

## References

- Beasley, A.J., D. Gordron, A.B. Peck, et al. 2002, *ApJS* 141, 13  
 Chavushyan, V., Mujica, R., Gorshkov, A. G., et al., 2001, *Astronomy Report*, Vol.45, No.2, 79  
 Cotton, W. D., Dallacasa, D., Fanti, C., Fanti, R., Foley, A. R., Schilizzi, R. T., Spencer, R. E., 2003, *A&A* 406, 43  
 de Vries, W. H., Barthel, P. D., O’Dea, C. P., 1997, *A&A* 321, 105  
 Dallacasa, D., Bondi, M., Alef, W., Mantovani, F., 1998, *A&AS* 129, 219  
 Dallacasa, D., Stanghellini, C., Centonza, M., Fanti, R., 2000, *A&A* 363, 887  
 Dallacasa, D., 2004, in the Proceedings of 7th European VLBI Network Symposium, eds: Bachiller, R., Colomer, F., Desmurs, J. F., de Vicente, P., p59  
 Fanti, C., Fanti, R., Dallacasa, D., Schilizzi, R. T., Spencer, R. E., Stanghellini, C., 1995, *A&A* 302, 317  
 Fanti, C., 2000, in the Proceedings of 5th European VLBI Network Symposium, held at Chalmers Technical University, eds. A. G. Polatidis, R. S. Booth, & Y. Pihlström (Published by Onsala Space Observatory), p73  
 Griffith, M., Langston, G., Heflin, M., Conner, S., Lehar, J., Burke, B., 1990, *ApJS* 74, 129  
 Guainazzi, M., Siemiginowska, A., Rodriguez-Pascual, P., and Stanghellini, C., 2004, *A&A* 421, 461  
 Gugliucci, N. E., Taylor, G. B., Peck, A. B., Giroletti, M., 2005, *ApJ* 622, 136  
 Heckman, T. M., O’Dea, C. P., Baum, S. A., Laurikainen, E., 1994, *ApJ* 428, 65  
 Homan, D. C., Attridge, J. M., Wardle, J. F. C., 2001, *ApJ* 556, 113  
 Kühr, H., Pauliny-Toth, I. I. K., Witzel, A., Schmidt, J., 1981, *AJ* 86, 6  
 Lister, M. L., Marscher, A. P., 1998, *ApJ* 504, 702  
 Lister M. L., Kellermann K. I., Vermeulen R. C., Cohen M. H., Zensus J. A., Ros E., 2003, *ApJ* 584, 135L  
 Murgia, M., Fanti, C., Fanti, R., Gregorini, L., Klein, U., Mack, K.-H., Vigotti, M., 1999, *A&A* 345, 769  
 Murgia, M., 2003, *PASA* 20, 19  
 O’Dea, C. P., Stanghellini, C., Baum, S. A., Charlot, S., 1996, *ApJ* 470, 806  
 O’Dea, C. P., 1998, *PASP* 110, 493  
 Orienti, M., Dallacasa, D., Tinti, S., Stanghellini, C., 2006, *A&A* in press

- Orienti, M., Dallacasa, D., Fanti, C., Fanti, R., Tinti, S., Stanghellini, C., 2004, *A&A* 426, 463
- Owsianik, I., Conway, J. E., 1998, *A&A* 337, 69
- Pearson, T. J., Readhead, A. C. S., 1988, *ApJ* 328, 114
- Petrov, L., Kovalev, Y. Y., Fomalont, E., Gordon D., 2005, *AJ* 129, 1163
- Polatidis, A. G., Conway, J. E., 2003, *PASA* 20, 69
- Scott, W. K., Fomalont, E. B., Horiuchi, S., Lovell, J. E. J., et al., 2005, *ApJS* 155, 33
- Snellen, I. A. G., Schilizzi, R. T., Miley, G. K., de Bruyn, A. G., Bremer, M. N., Röttgering, H. J. A., 2000, *MNRAS* 319, 445
- Stanghellini, C., O'Dea, C. P., Dallacasa, D., Cassaro, P., Baum, S. A., Fanti, R., Fanti, C., 2005, *A&A* 443, 891
- Stanghellini, C., O'Dea, C. P., Baum, S. A., Laurikainen, E., 1993, *ApJS* 88, 1
- Stanghellini, C., O'Dea, C. P., Dallacasa, D., Baum, S. A., Fanti, R., Fanti, C., 1998, *A&AS* 131, 303
- Stanghellini, C., Dallacasa, D., Bondi, M., Xiang, L., 2000, in the Proceedings of 5th European VLBI Network Symposium, held at Chalmers Technical University, eds. A. G. Polatidis, R. S. Booth, & Y. Pihlström (Published by Onsala Space Observatory), p99
- Stickel, M., Kühr, H., 1994, *A&AS* 103, 349
- Stickel, M., Kühr, H., 1996, *A&AS* 115, 1
- Spoelstra, T. A. T., Patnaik, A. R., Gopal-Krishna, 1985, *A&A* 152, 38
- Taylor, G. B., Peck, A. B., 2003, *ApJ* 597, 157
- Vermeulen, R. C., Pihlström, Y. M., Tscharger, W., et al., 2003, *A&A* 404, 861
- Wright, A. and Otrupcek, R., Parkes Catalogue, 1990, Australia Telescope National Facility
- Xiang, L., Stanghellini, C., Dallacasa, D., Haiyan, Z., 2002, *A&A* 385, 768
- Xiang, L., Dallacasa, D., Cassaro, P., Jiang, D., Reynolds, C., 2005, *A&A* 434, 123
- Xu, W., Readhead, A. C. S., Pearson, T. J., Polatidis, A. G., Wilkinson, P. N., 1995, *ApJS* 99, 297
- Yang, J., Liu, X., 2005, *ChJAA*, Vol.5, Suppl., 224

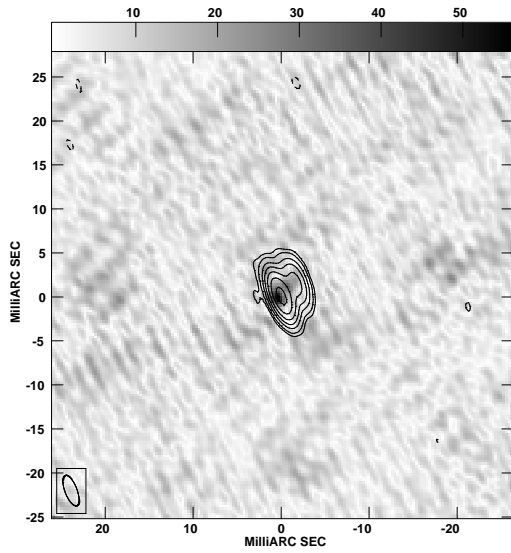


**Fig. 1.** DA193 at 5 GHz, the restoring beam is  $3.7 \times 1.4$  mas in PA  $21.0^\circ$ , the contours are total intensity with 34 mJy/beam times -2, -1, 1, 2, 5, 10, 20, 40, 80, and the peak of 3433 mJy/beam. The overlay in grey is linearly polarized intensity, with the peak of 56 mJy/beam.

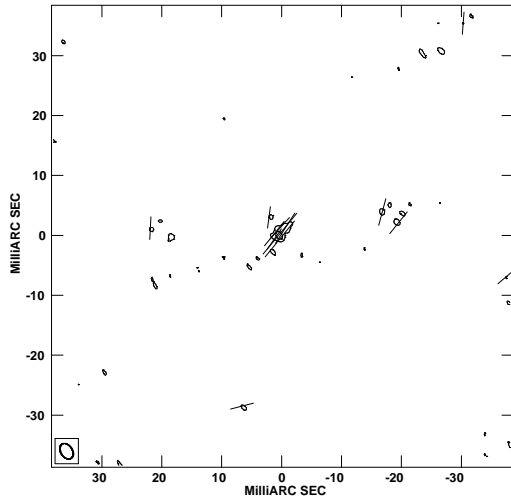


**Fig. 2.** Linear polarization map of DA193 with polarization angle superimposed at 5 GHz, the restoring beam is  $2.8 \times 1.9$  mas in PA  $32.5^\circ$ , the contours are 20 mJy/beam times -2, -1, 1, 2, with the peak of 56 mJy/beam.

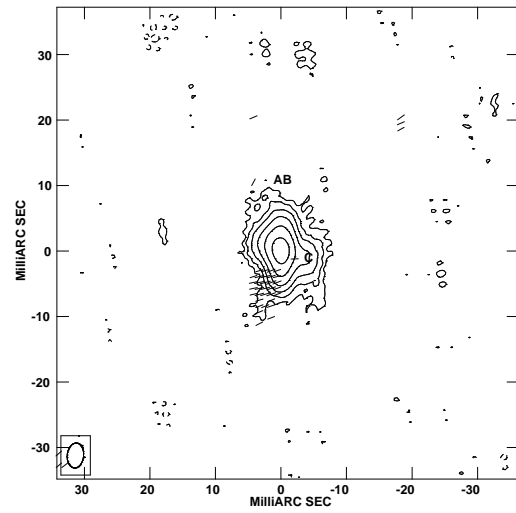


**Fig. 3.** 0554-026 at 5 GHz, the restoring beam is  $3.8 \times 2.5$  mas in PA  $-5.8^\circ$ , the contours are 1.5 mJy/beam times -2, -1, 1, 2, 4, 8, 16, 32, with the peak of 71 mJy/beam. The electric vectors of possible polarizations are superimposed.

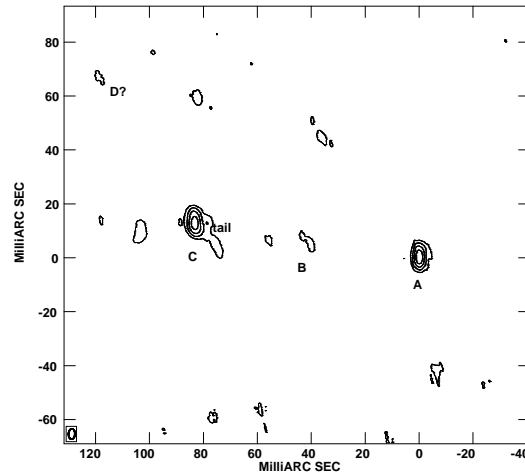


**Fig. 4.** 0914+114 at 5 GHz, the restoring beam is  $4.7 \times 2.9$  mas in PA  $-1.5^\circ$ , the contours are 1.6 mJy/beam times -2, 1, 2, 4, 8, with the peak of 28 mJy/beam.

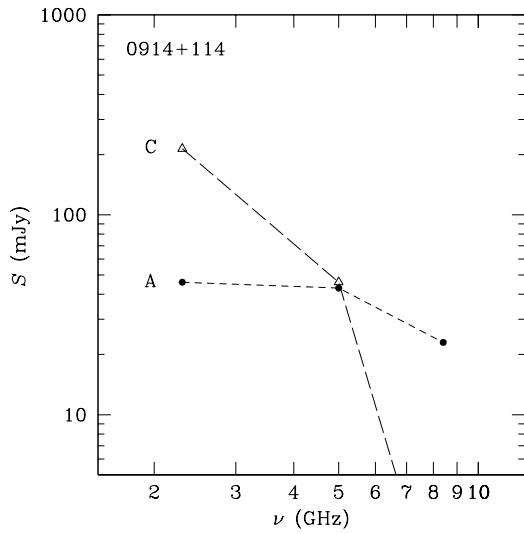


**Fig. 5.** Component spectra of source 0914+114 from the VLBI data at 2.3, 5.0, and 8.4 GHz, where flux of component C at 8.4 GHz is  $\leq 1$  mJy.

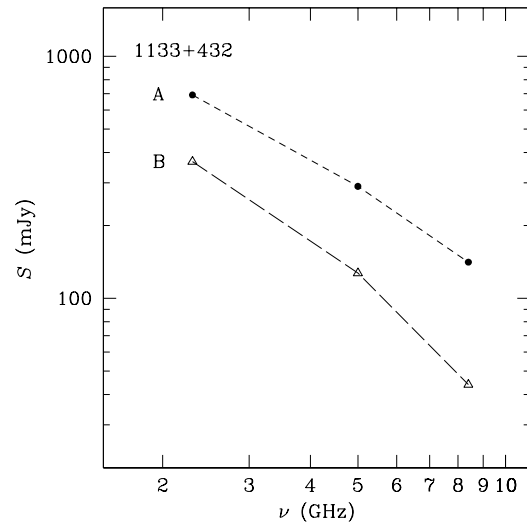


**Fig. 7.** Component spectra of source 1133+432 from the VLBI data at 2.3, 5.0, and 8.4 GHz

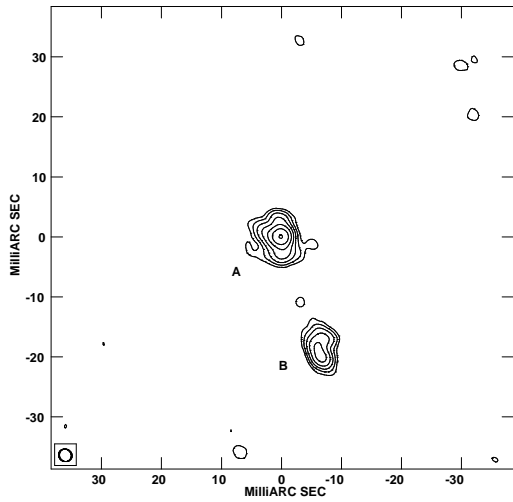


**Fig. 6.** 1133+432 at 5 GHz, the restoring beam is  $2.2 \times 2.0$  mas in PA  $51^\circ$ , the contours are 1.5 mJy/beam times -2, -1, 1, 2, 4, 8, 16, 32, 64, with the peak of 134 mJy/beam.

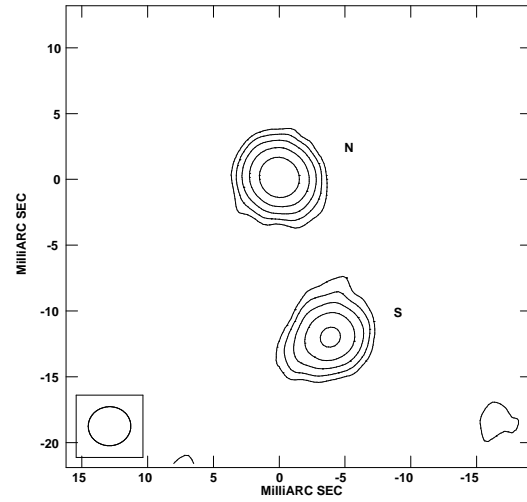


**Fig. 8.** 1333+589 at 5 GHz, the restoring beam is  $3.2 \times 3.0$  mas in PA  $-87^\circ$ , the contours are 10 mJy/beam times -2, 1, 2, 4, 8, 16, with the peak of 290 mJy/beam.

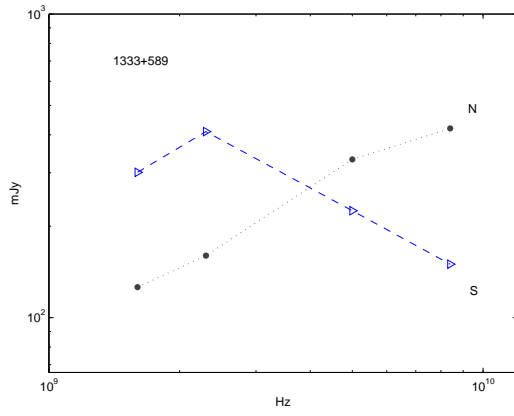


**Fig. 9.** Component spectra of source 1333+589 from the VLBI data at 1.6, 2.3, 5.0, and 8.4 GHz

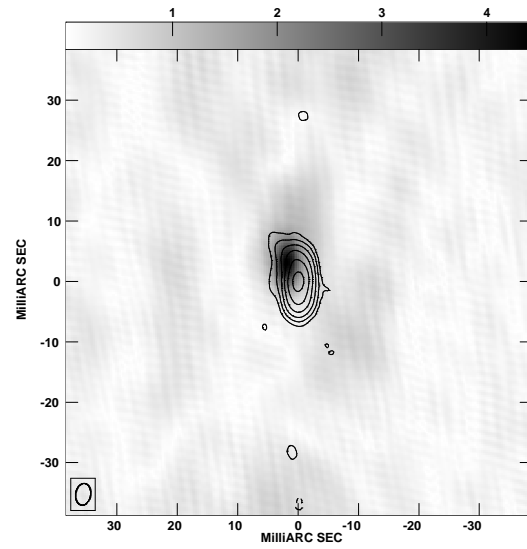


**Fig. 11.** 1433-040 at 5 GHz, the restoring beam is  $3.6 \times 2.5$  mas in PA  $-8.6^\circ$ , the contours are total intensity with 2.0 mJy/beam times -2, 1, 2, 4, 8, 16, 32, 64, 90, and the peak of 84.2 mJy/beam. The overlay in grey is linearly polarized intensity, with the peak of 3.8 mJy/beam.

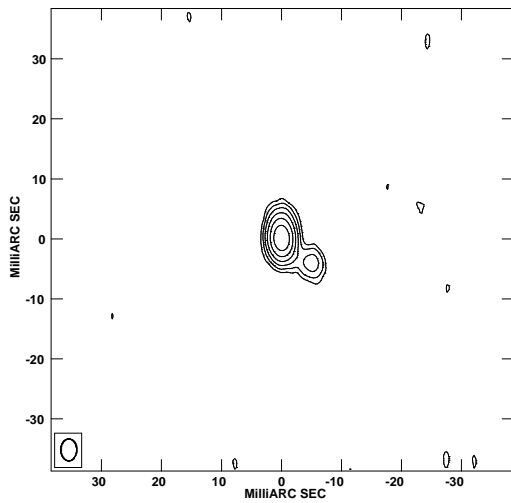


**Fig. 10.** OQ208 at 5 GHz, the restoring beam is  $3.7 \times 2.6$  mas in PA  $0^\circ$ , the contours are 20 mJy/beam times -2, 1, 2, 4, 8, 16, 32, 64, with the peak of 1749 mJy/beam.

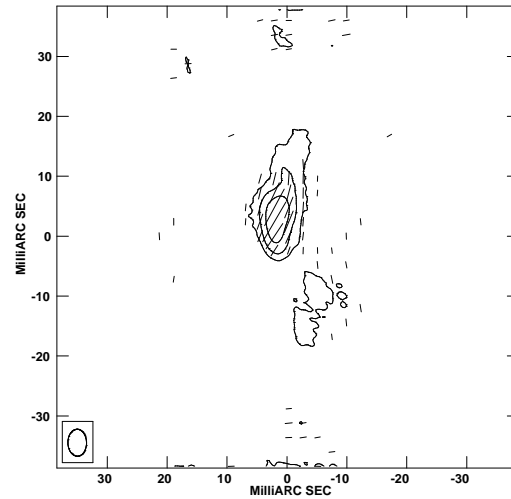


**Fig. 12.** Linear polarization map of 1433-040 with polarization angle superimposed at 5 GHz, the restoring beam is  $5.0 \times 3.4$  mas in PA  $1.8^\circ$ , the contours are 0.5 mJy/beam times -2, -1, 1, 2, 4, with the peak of 3.8 mJy/beam.

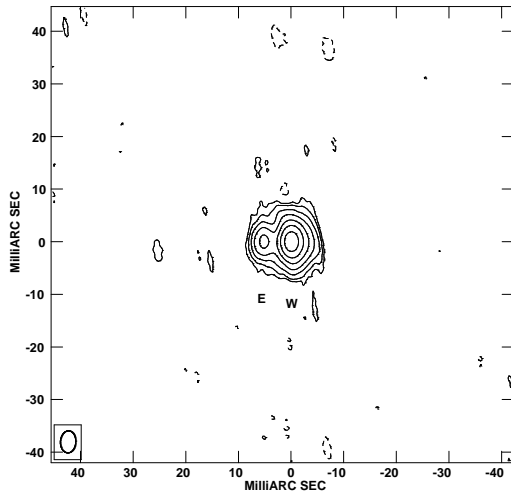


**Fig. 13.** 1509+054 at 5 GHz using uniform weighting with an AIPS robust parameter of 1, the restoring beam is  $4.2 \times 2.94$  mas in PA  $-3.3^\circ$ , the contours are 4 mJy/beam times -2, -1, 1, 2, 4, 8, 16, 32, 64, with the peak of 407 mJy/beam.

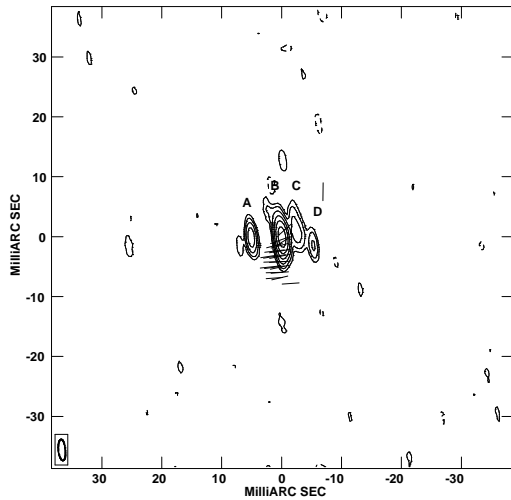


**Fig. 14.** 1509+054 at 5 GHz using uniform weighting with an AIPS robust parameter of -2, the restoring beam is  $3.6 \times 1.2$  mas in PA  $5.2^\circ$ , the contours are 6 mJy/beam times -2, -1, 1, 2, 4, 8, 16, 32, with the peak of 325 mJy/beam. The electric vectors of possible polarizations are superimposed.

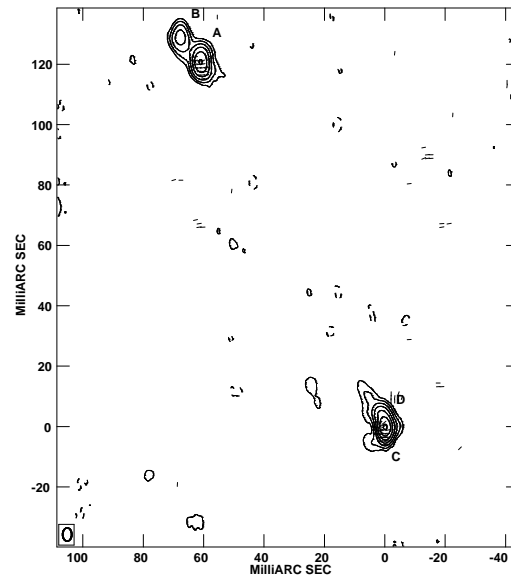


**Fig. 15.** 1518+046 at 5 GHz, the restoring beam is  $4.4 \times 3.0$  mas in PA  $-0.3^\circ$ , the contours are 4 mJy/beam times -2, -1, 1, 2, 4, 8, 16, 32, 64, with the peak of 276 mJy/beam. The electric vectors of possible polarizations are superimposed.

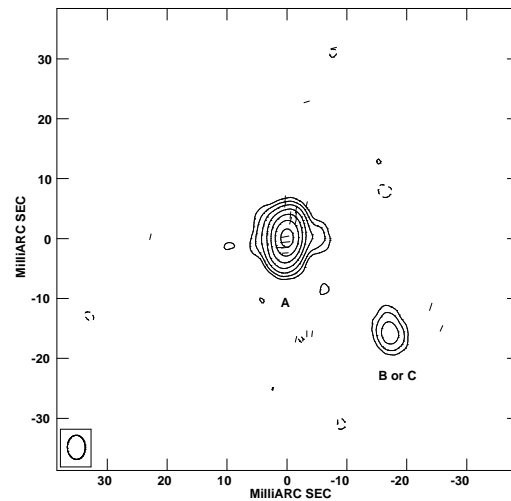


**Fig. 16.** 1751+278 at 5 GHz, the restoring beam is  $4.1 \times 3.0$  mas in PA  $1.8^\circ$ , the contours are 2.0 mJy/beam times -2, -1, 1, 2, 4, 8, 16, 32, 64, with the peak of 170 mJy/beam. The electric vectors of possible polarizations are superimposed.

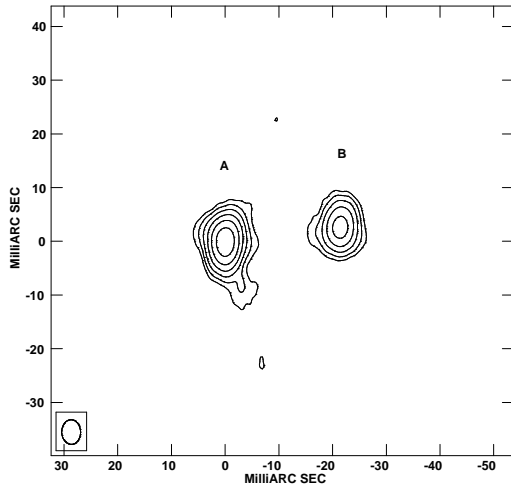


**Fig. 17.** 1824+271 at 5 GHz, the restoring beam is  $4.6 \times 3.5$  mas in PA  $1.7^\circ$ , the contours are 0.9 mJy/beam times -2, 1, 2, 4, 8, 16, 32, with the peak of 50 mJy/beam.

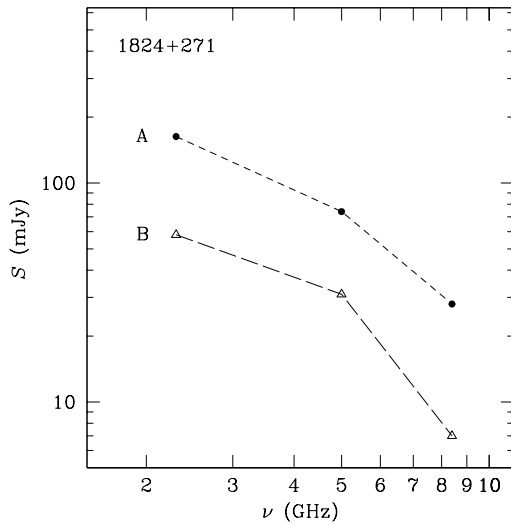


**Fig. 18.** Component spectra of source 1824+271 from the VLBI data at 2.3, 5.0, and 8.4 GHz

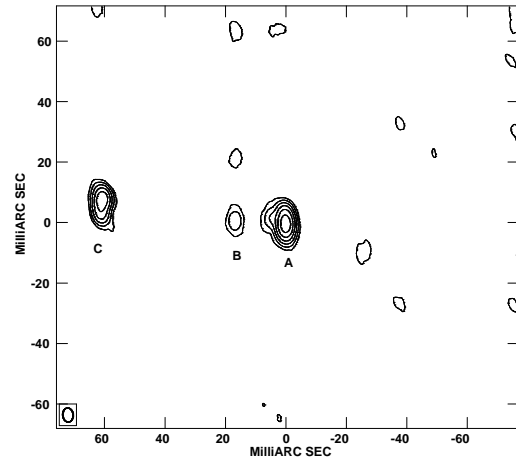


**Fig. 19.** 2121-014 at 5 GHz, the restoring beam is  $4.7 \times 3.4$  mas in PA  $4.9^\circ$ , the contours are 2 mJy/beam times -2, 1, 2, 4, 8, 16, 32, with the peak of 107 mJy/beam.

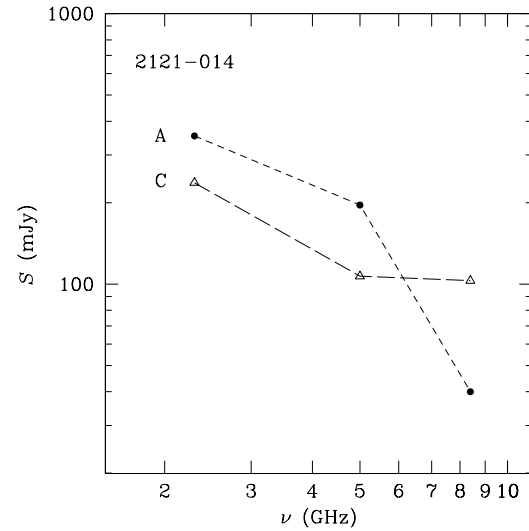


**Fig. 20.** Component spectra of source 2121-014 from the VLBI data at 2.3, 5.0, and 8.4 GHz

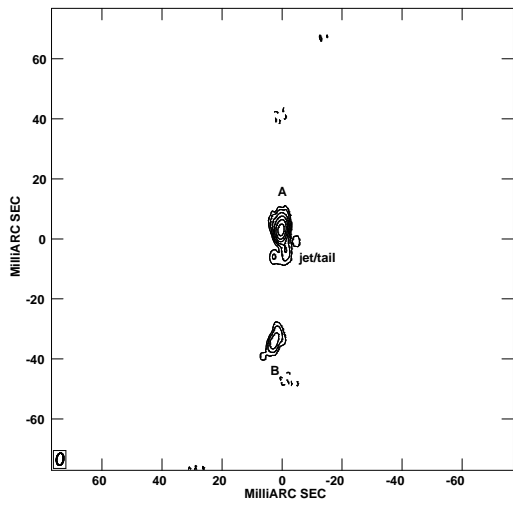


**Fig. 21.** 2322-040 at 5 GHz, the restoring beam is  $4.0 \times 2.3$  mas in PA  $-7.6^\circ$ , the contours are 6 mJy/beam times -2, 1, 2, 4, 8, 16, 32, with the peak of 299 mJy/beam.

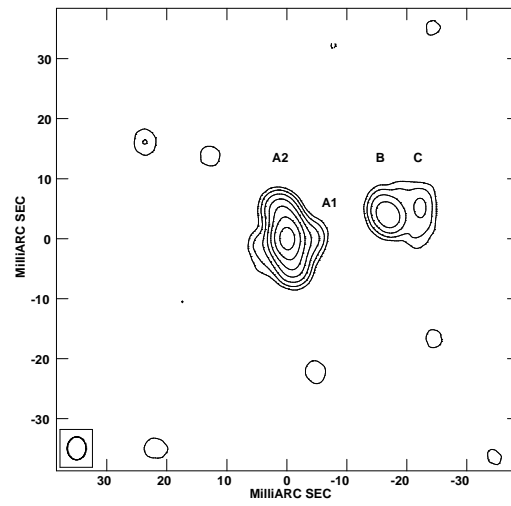


**Fig. 23.** 2323+790 at 5 GHz, the restoring beam is  $3.8 \times 3.1$  mas in PA  $-1.6^\circ$ , the contours are 2 mJy/beam times -2, 1, 2, 4, 8, 16, 32, 64, with the peak of 184 mJy/beam.

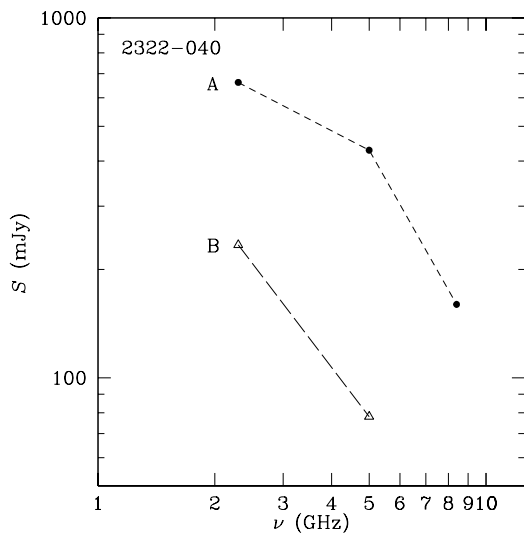


**Fig. 22.** Component spectra of source 2322-040 from the VLBI data at 2.3, 5.0, and 8.4 GHz